Experimental Mechanics (2013) 53:1735–1742
DOI 10.1007/s11340-013-9748-z

Thin and Thermally Stable Periodic Metastructures

E. Gdoutos · A.A. Shapiro · C. Daraio

Received: 9 January 2013 / Accepted: 2 April 2013 / Published online: 18 May 2013
© Society for Experimental Mechanics 2013

Abstract We design, fabricate, and test thin thermally stable metastructures consisting of bi-metallic unit cells and show how the coefficient of thermal expansion (CTE) of these metastructures can be finely and coarsely tuned by varying the CTE of the constituent materials and the unit cell geometry. Planar and three-dimensional finite element method modeling (FEM) is used to drive our design and inform experiments, and predict the response of these metastructures. We develop a robust experimental fabrication procedure in order to fabricate thermally stable samples with high aspect ratios. We use digital image correlation (DIC) and an infrared camera to experimentally measure displacement and temperature during testing and compute the CTE of our samples. The samples, composed of an aluminum core and an external titanium frame, exhibit a CTE of 2.6 ppm/°C, which is significantly lower than either constituent. These unit cells can be assembled over a large area to create thin low-CTE foils. Finally, we demonstrate how the approach developed in this work can be used to fabricate metastructures with CTE's ranging from −3.6 ppm/°C to 8.4 ppm/°C.

Keywords Low thermal expansion · Thermally stable · Tunable CTE · Metastructures · bi-metallic array

E. Gdoutos · C. Daraio (✉)
Graduate Aerospace Laboratories,
California Institute of Technology, Pasadena, CA 91125, USA
e-mail: daraio@caltech.edu

A.A. Shapiro
Jet Propulsion Laboratory, California Institute of Technology,
4800 Oak Grove Dr.,
Pasadena, CA 91109, USA

Introduction

Designing materials with engineered specified thermal expansion (CTE) has significant applications in biomedical engineering, semiconductors, and solar energy. It is particularly important to combine a desired (usually low) CTE with mechanical robustness at thin scales [1, 2]. Work has been conducted to develop thin materials with low thermal expansion for use in biomedical applications [1], flexible circuit boards and electronics packaging [3, 4], and flexible solar cells [5]. Most of this previous work has been focused on designing low-CTE materials by modifying compounds at the atomic level or by using the low CTE of fiber structures to constrain the thermal expansion of an overall matrix, such as in composites. It is also possible to design metastructures with specific CTE by selecting the topology of different constituent materials [6, 7]. These metastructures work by releasing thermal strain in open spaces while exhibiting areas of minimal displacement, thus exhibiting low overall CTE. Even negative CTE metastructures can be readily attained [6]. Theory has been developed to predict their thermal behavior [6–9] and a few examples have been experimentally realized [9–11]. Their mechanical stiffness and transient and steady state thermal response have been characterized [9, 10]. Investigation of the mechanical and thermal behavior at the interface between the two constituent materials has also been conducted experimentally and computationally [10]. In addition, Berger et al. [12] developed detailed design principles for low thermal expansion structures and studied their in-plane buckling behavior. Recently, work has been conducted on utilizing such structures in acreage thermal protection systems for hypersonic vehicles [11]. However, the previous work on low CTE metastructures demonstrated the applicability of the design principles only in large, macroscale structures [11, 12]. Furthermore, previous computational models [11, 12] do not take into account 3D effects. These effects become significant in

high-aspect ratio metastructures, where the two constituent materials overlap at the joints. In this work, we build and test thin (<200 μm), tunable CTE metastructures with large aspect ratios (~100). In addition to fabricating metastructures that are 25 times thinner than in [12] and potentially leading to highly flexible metastructures, we build on previous work in the following ways: (i) We study, quantify, and exploit the effect on the CTE of additional realistic design parameters (e.g. frame beam width, young's moduli, contact area); (ii) we improve the interface of the constituent materials to optimize fabrication procedures allowing further scaling down of these metastructures; (iii) we perform a complete study of the effects of out-of-plane deformations; (iv) we develop a predictive model including a sensitivity analysis. Our structures are well suited for applications where low thickness, high aspect ratio, and mechanical flexibility are desirable, such as biomedical devices, solar energy systems, and semiconductors. The large aspect ratio of the metastructures in our design causes sensitivity to stress concentration. To manage these stresses we add curvature to the unit cell near the regions of least in-plane displacement. We model the metastructures using both planar and full three-dimensional finite element models to guide the experimental design of the materials interfaces and to inform the experiments.

In order to design a thin and thermally stable unit cell we draw inspiration from previous theoretical work [9] as a starting point and employ FEM simulations to drive our design process. In 2007, Steeves et al. [9] showed that through a specific periodic arrangement in a two-dimensional truss-like structure of two pin jointed materials with different CTE's (Fig. 1(a)) the overall response of the structure could have zero CTE at specific points. The thermal expansion of these points is governed by equation (1) [9]:

$$\alpha = \alpha_1 \frac{1 - \frac{1}{2}\left(\frac{\alpha_2}{\alpha_1}\right)\sin(2\theta)\left(\frac{1}{\sqrt{3}} + \tan(\theta)\right)}{1 - \frac{1}{2}\sin(2\theta)\left(\frac{1}{\sqrt{3}} + \tan(\theta)\right)}, \quad (1)$$

where α is the CTE of the overall structure, α_1 and α_2 are the CTE's of the constituent low CTE and high CTE materials respectively, and θ is a characteristic angle of the unit cell. As can be seen in equation (1), the overall CTE of the structure is a function of the ratio of CTE's of the constituents and the characteristic angle θ. As shown in Fig. 1, this function vanishes for pairs of values of θ and α_2/α_1. Thus by designing a unit cell with specific angle θ and picking appropriate constituent materials, it is possible to create unit cells, and consequently full-scale lattices having a final CTE less than that of either constituent.

Design and Computational Method

General Design Principles

In this study, the unit cell is composed of an outer frame (Fig. 2(a)) and an inner plate (Fig. 2(b)) combined to form a low CTE metastructure (Fig. 2(c)), as in [12]. However, the unit cells presented here are ~25 times thinner, ~4 times smaller laterally, and have ~6 times higher aspect ratio than those in [12]. Such smaller sizes required the redesign of the interface between the constituent materials, to mitigate fabrication challenges. The interfaces of the two constituents are lap-jointed and ultimately fabricated by spot laser-welding instead of press fit jointed as in [12]. This unit cell can also be extended to a full-scale lattice, shown schematically in Fig. 2(d) and as experimentally fabricated in Fig. 2(e).

The plate and frame are joined at three interfaces. These interfaces displace primarily in-plane during thermal loading and cause rotation but no in-plane displacement, at the low-CTE points (Fig. 2(c, d)). In this design, the characteristic angle θ is fixed at 30°. This results in the frame having a regular hexagonal shape, which is advantageous for isotropy in mechanical and thermal response. Unit cell dimensions are as shown in Fig. 2(c) with thickness of 125 μm. Lateral dimensions are chosen by taking into account functional, application, and fabrication based constrains. To understand the behavior of these structures and predict their thermal and mechanical response we build realistic FEM models. While previous theoretical work [9, 12] has provided significant insight to the thermal response, it is based on several approximations: (i) parts are composed of truss members; (ii) the interfaces are point contact; (iii) the interfaces are either pinned or bonded (iv) it does not take into account out-of-plane effects which are relevant for this design. In addition, it gives little insight into the response of the structure as a function of variables other than θ and α_2/α_1.

Thermal Response

We conduct planar and full 3D FEM models of a metastructure as shown in Fig. 2(c). In the planar case, to account for the high aspect ratio and low thickness of the structure, we model the structure using triangular shell elements. In the full 3D case, we use 10 node tetrahedral elements. The interface between the plate and the frame is modeled as bonded. The main simplification of the planar model is that the two constituent parts of the unit cell are modeled in the same plane, whereas the 3D model fully captures the geometry of the metastructure. We compute displacements under the application of a thermal load of 80 °C (Fig. 3). We calculate the CTE of the unit cell by looking at the expansion of the low-CTE points (indicated by arrows in Fig. 2(c and d)) and perform this analysis for

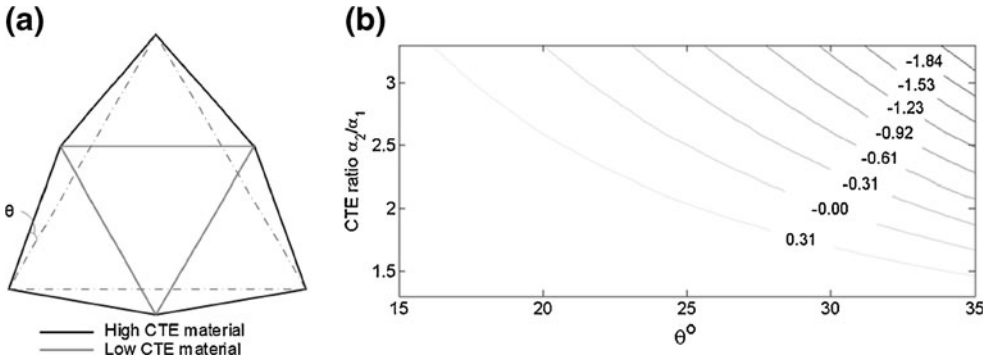

Fig. 1 (**a**) Pin-jointed structure designed by Steeves [9] consisting of a high CTE and a low CTE material and exhibiting low overall CTE, governed by equation (1). (**b**) equation (1) plotted for various values of $\boldsymbol{\alpha}_2/\boldsymbol{\alpha}_1$ and θ showing the thermal expansion coefficient of a pin jointed low CTE structure [9] normalized by $\boldsymbol{\alpha}_1$. It is possible to achieve zero and even negative thermal expansion coefficient by picking appropriate combinations of CTE ratio $\boldsymbol{\alpha}_2/\boldsymbol{\alpha}_1$ and angle θ

multiple values of design variables (Fig. 3). The 3D FEM predicts higher CTE for the unit cell than the planar FEM model. For a metastructure composed of constituents with CTE ratio of 2.7, and frame width of 814 μm (the design that was experimentally implemented and discussed in "Experimental, Results, and Discussion"), the planar FEM model predicts a CTE of 0.6 ppm/°C, while the full 3D FEM model predicts a CTE of 1.19 ppm/°C. As shown in "Measurement of the Thermal Expansion Coefficient", the full 3D FEM prediction agrees better with experimental results.

In order to understand the response of the metastructure as well as the limitations of this approach, we study its thermal response as a function of two design variables: (i) the ratio of CTE's of the constituents; (ii) the frame width normalized by the length of the unit cell (12.4 mm). We consider CTE ratios between 1.75 and 2.75. We study this range because the CTE ratio of most metals is below 2.75 [13] and at ratios less than 1.75 the CTE of the unit cell is higher than desired. As seen in Fig. 3, the CTE ratio has a significant effect on the unit cell CTE, as predicted by equation (1).

To study the effects of the unit cell's geometry, we model frames with normalized widths between 3.84×10^{-2} (476 μm frame width) and 10.97×10^{-2} (1.36 mm frame width). These widths ratios were selected based on bounds imposed by fabrication constraints on the lower end and the resulting CTE of the unit cell on the high end. As the normalized width dimension increases, the CTE of the unit cell increases. This is due to increased resistance in the bending of the frame. Furthermore, it is evident from Fig. 3 that equation (1) is not a good approximation for the CTE of the unit cell. This is most likely due to violation of the assumption that the frame's beams behave like truss structures. This presents a design trade-off as the frame beams need to be wide enough to support structural loads, but the ratio of CTE's of the constituent materials needs to be small

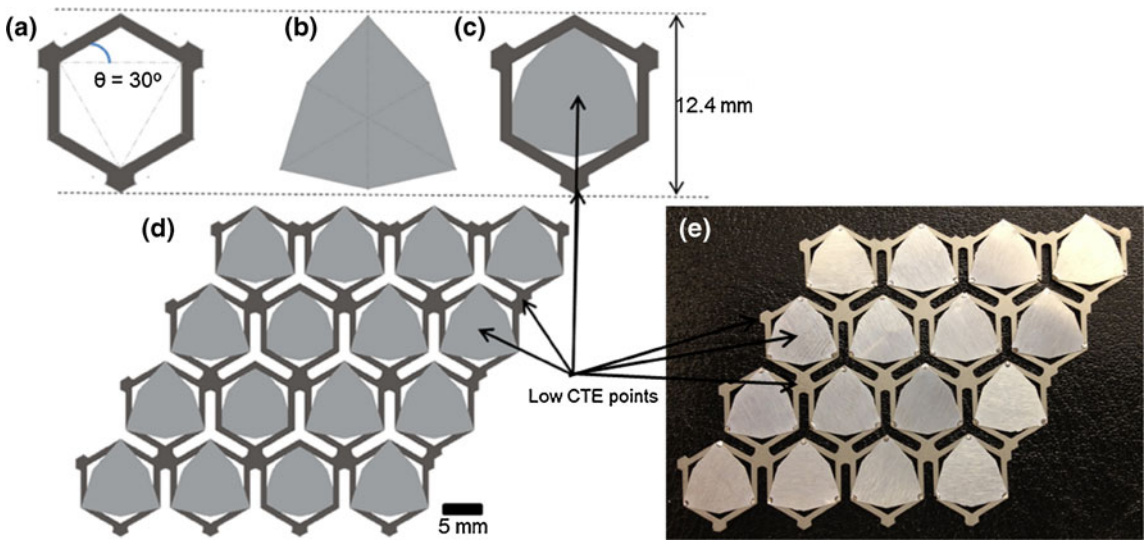

Fig. 2 (**a**) Schematic diagram showing the geometrical characteristics of the unit cell's outer frame. (**b**) Schematic diagram of the unit cell's inner plate. (**c**) Schematic diagram of the assembled unit cell. (**d**) Lattice exhibiting low CTE over wide area. (**e**) Experimentally fabricated lattice

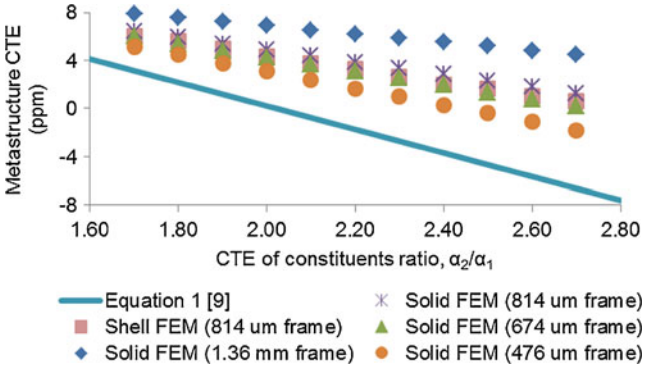

Fig. 3 The CTE of the unit cell as predicted by FEM for various CTE ratios α_2/α_1. The *solid line* indicates the prediction of equation (1). The *circular, triangular, star, and rhomboidal symbols* indicate the FEM prediction of a unit cell design with frame width ratios of 3.84×10^{-2}, 5.44×10^{-2}, 6.56×10^{-2}, and 10.97×10^{-2}, respectively. The *square symbols* indicate the planar FEM prediction of the 6.56×10^{-2} frame width ratio unit cell. The full 3D solid FEM model predicts a higher CTE for the unit cell than the planar FEM model

to prevent significant dissimilarities between the two materials which would result in fabrication challenges. In the final design selected for experimental testing, the normalized frame width is 6.56×10^{-2} (814 μm frame width). We chose this frame width as it results in a design with the lowest beam width still ensuring structural stability of the structure, scalability to smaller scales, and fabrication feasibility in the current scale. The existing theoretical framework for these metastructures treats all constituent materials as beams. In this work, we computationally compare the response of a metastructure consisting of all beam elements (as in the theoretical framework) and of one with a plate interior constituent, using FEM. Detailed analysis (not shown here) yielded negligible difference in the thermal response of the two unit cells.

Out-of-Plane Effects

In addition to in-plane geometrical effects, out-of-plane deformation is particularly important to this design. The thin scale and relative out-of-plane attachment of the constituent parts can induce out-of-plane deformation on the cells. A potential application of this low CTE structure is as a thermally stable layer in an active mirror layup [14]. In this scenario, the out-of-plane response of this metastructure is critical to the performance of the optics. Figure 4(a) shows the maximum out-of-plane deformation induced during thermal loading as a function of unit cell thickness, as predicted by 3D FEM. As the thickness decreases, the out-of-plane deformation increases, exhibiting the importance of out-of-plane effects, at thinner scales.

Figure 4(b) shows the effect of thickness on the CTE of the unit cell. As the thickness increases from 50 μm to 250 μm the CTE also increases, from 0.92 to 1.49 ppm/°C. The dependence of CTE on thickness suggests that the out-of-plane deformation has a measurable impact on the CTE of the metastructure. However, this impact is small and does not influence the low-CTE performance of the metastructure.

Experimental, Results, and Discussion

Sample Fabrication and Measurement Setup

With the final frame width selected in our experiments and having verified that out-of-plane deformations will not severely negatively impact the CTE of this metastructure, we proceeded to experimentally show that this metastructure indeed behaves as predicted. While we intend to experimentally show metastructures achieving different (and even negative) values of CTE in the future, in this work we focus on showing near-zero CTE. Thus, based on Fig. 3, we chose to experimentally realize this design with two materials whose CTE ratio is about 2.7. Based on their CTE ratio and mechanical robustness, we fabricated the outer frame out of Titanium (α_{Ti}=8.6 ppm) and the inner plate out of Aluminum (α_{Al}=23.1 ppm) [13].

We fabricated and prepared samples for testing in three steps: (i) fabricate the Ti frame and Al plate separately; (ii) attach the two pieces at three points; (iii) add speckle pattern for DIC [15, 16] testing. Frame and plates were fabricated using wire electron discharge machining (EDM). Figure 5(a) shows a unit cell after the laser welding step, but before the speckle pattern has been applied. Following fabrication the two parts were cleaned and attached at three points by laser welding (Fig. 5(b)). Laser welding was performed with a 50 W maximum power pulsed Nd:YAG laser. During the laser welding process, the laser beam is normal to the sample while Argon gas was used to remove oxygen from the weld area. Finally, a speckle pattern was added by first painting the sample white and then adding black speckles by spray painting. From a random sample of speckles, the average speckle size was 26.97 pixels. Approximately half of the speckles contained less than 20 pixels and 40 % of speckles contained 10–20 pixels. The size was controlled by changing the distance from which black spray paint was applied. The speckle size must be large enough to prevent aliasing but small enough that the correlation algorithm can accurately track the speckle subsets. The DIC algorithm tracks the speckle pattern by performing a correlation on the greyscale values of "subsets" (groups of pixels) between the deformed and undeformed images. Based on the correlation, displacements are computed at specific pixels, with the resolution determined by the "step" size (e.g., with a step size of 1, displacements are computed at every pixel). If the step size

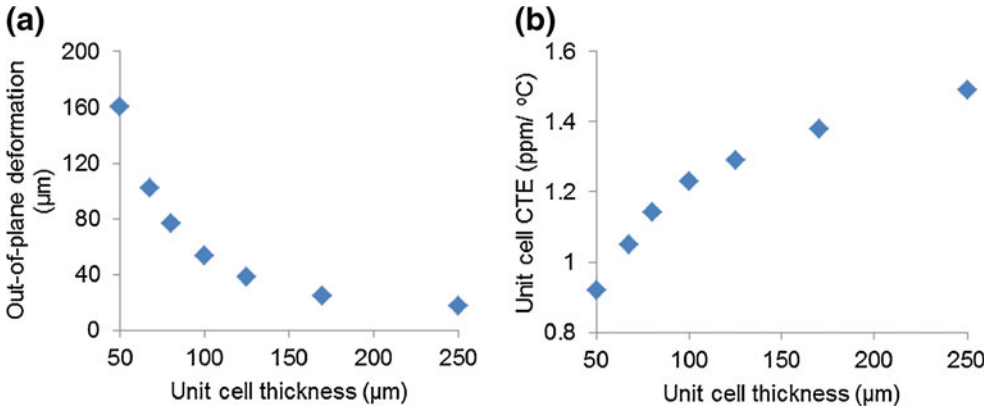

Fig. 4 (**a**) The maximum out of plane deformation of a unit cell as a function of the unit cell's thickness. The maximum out of plane deformation occurs at the frame's regions of least in-plane displacement; (**b**) The CTE of a unit cell as a function of the unit cell's thickness. There is a measurable decrease in the CTE as the thickness decreases

is too high, spatial resolution is lost; if it is too low, noise is introduced to the displacement field. Subsets in this work were composed of 21 pixels and the step size was 5 pixels. This resulted in a ~50 μm spatial resolution and a correlation displacement accuracy of ~500 nm. The correlation accuracy corresponds to ~5 % of the maximum displacement observed. The 50 μm spatial resolution is adequate to capture the overall deformation behavior of the ~12 mm sample.

We experimentally measured the CTE of the samples by heating them and measuring displacements using DIC. The samples were heated on a hot plate and the temperature was measured using an infrared camera, a thermocouple, and a resistance temperature detector. The IR camera used in this work, a FLIR SC6000, employs an indium-antimonide detector, sensitive at 3–5 μm [17]. The IR camera's reading was verified with thermocouples between room temperature and 250 °C and was found accurate to within 0.4 °C. To achieve such accuracy it is necessary that the emissivity of objects imaged is high enough (ε>0.9) so that the radiation from the sample is detectable against noise. The objects being imaged during thermal testing were the aluminum plate on top of the hot plate and the arrays composed of aluminum and titanium. The emissivity of these materials generally ranges from 0.04 to 0.2 [18], which is too low for accurate temperature reading. This was resolved however, by spray painting the objects with Krylon Flat Black 1502 (ε=0.95) [19]. Images were taken once the temperature had stabilized at steps between 40 °C and 160 °C using a Nikon ShuttlePix P-400R microscope. We then computed the displacements at each temperature step using commercial VIC-2D [20] software.

Measurement of the Thermal Expansion Coefficient

We observed agreement between the deformation predicted by our full 3D FEM model and the experimentally tested samples (Fig. 6). The four thermally stable areas predicted by the FEM models (shown in colder/darker color tones in Fig. 6(a, b)) agree very well with the low CTE areas in the experiments (Fig. 6(c)). The experimental data shows slight variations between the deformation at the welds, likely due to sample fabrication defects.

To validate our experimental setup we measured the CTE's of the fabricated Al and Ti parts by themselves. As shown in Fig. 7(a), we measured the CTE's of Al and Ti to be within

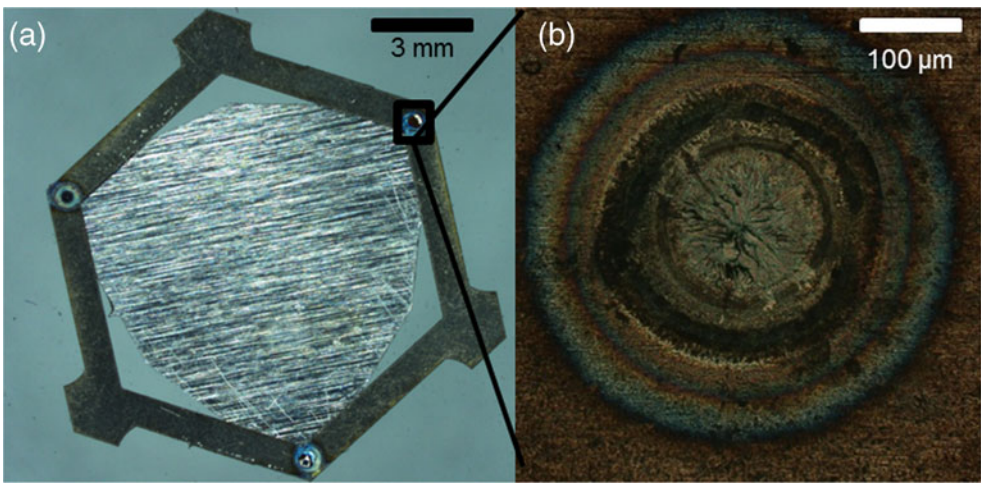

Fig. 5 (**a**) Fabricated low CTE sample comprised of an Al inner plate and a Ti outer frame; (**b**) Laser-welded interface between the sample's Al and Ti part

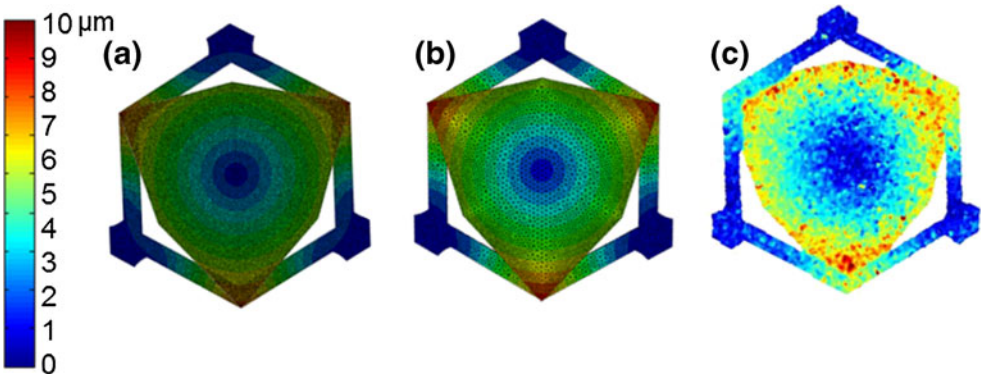

Fig. 6 Magnitude of in-plane deformation predicted for a 70 °C change in temperature by (**a**) planar FEM, (**b**) 3D FEM, and (**c**) experimentally observed between 55 °C and 125 °C. *Colder/darker color tones* represent regions of the unit cell with low thermal expansion

2.2 % and 1.6 % of values reported in literature [13], respectively. We measured our metastructures to have CTE of 2.56 ppm/°C (Fig. 7(a)). In Fig. 7(a), specifically for the unit cell, error bars with horizontal caps indicate one standard deviation in measurement of the CTE error, while error bars without horizontal caps indicate the predicted effect a 5 % measurement error in Al CTE, Ti CTE and frame width would have on the unit cell CTE.

CTE Tunability and Sensitivity Analysis

To demonstrate CTE tunability with this design, establish the effect of measurement error on our experimental results, and determine the sensitivity of the CTE to its dependent variables, we performed a sensitivity analysis on the CTE as a function of six parameters: the CTE's and elastic moduli of the constituents (α_1, α_2, E_1, E_2) and the width of the frame (f_{width}) and the size of the welded contact area ($A_{contact}$). The frame width and contact area were normalized by the unit cell length (as shown in Fig. 2(c)) to allow scaling. The welded contact area is neither a pivot nor a point contact, as assumed in equation (1). Thus, some deviation from the CTE predicted by equation (1) is expected. To assess the effect of the bending induced by the welded area, we analyze the sensitivity of the CTE to the contact area and frame width, in addition to the material properties. The sensitivity analysis indicated that a 5 % measurement error in the CTE of the materials, and frame width can lead to significant error in the unit cell CTE. This is shown as the error bars without horizontal caps on the unit cell in Fig. 7(a). Figure 7(b) shows the CTE of the unit cell as a function of frame width and the CTE of the inner plate constituent material. By varying those two parameters, it is possible to tune the CTE of the unit cell from −0.5 to 1 ppm/°C.

The sensitivity analysis was performed by running planar FEM simulations and computing the unit cell CTE by varying six parameters: α_1 from 7.6 to 9.6 ppm, α_2 from 22.1 to

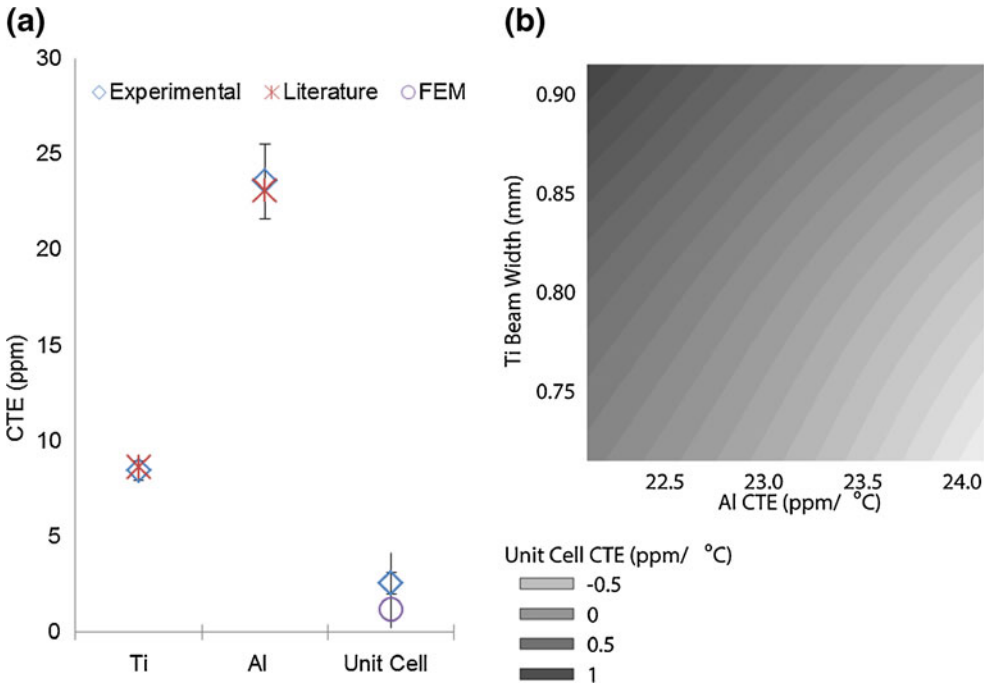

Fig. 7 (**a**) CTE of Ti, Al, and unit cell samples as measured by our setup. *Error bars* indicate one measurement standard deviation for Al and Ti. (**b**) Unit cell CTE as a function of frame width ('y' axis) and CTE of constituent material ('x' axis). The unit CTE can range from −0.5 to 1 ppm/°C ppm by adjusting the CTE of one of its constituents and the width of the other constituent

Table 1 Correlation coefficient between unit cell CTE and design parameters

α_1	α_2	f_{width}	$A_{contact}$	E_1	E_2
0.89	−0.33	0.29	0.04	0.03	−0.05

Table 2 CTE of metastructures with different constituent materials

Constituent 1 Constituent 2	Kovar Aluminum	Titanium Aluminum	Nickel Aluminum
CTE prediction (ppm/°C)	−3.63	1.12	8.35

24.1 ppm, E_1 from 106 to 126 GPa, E_2 from 60 to 80 GPa, f_{width} from 5.77×10^{-2} to 7.38×10^{-2} μm/μm, and $A_{contact}$ from 8.06×10^{-3} to 24.2×10^{-3} μm/μm. Then, commercial data analysis software JMP [21] was used to determine the correlation coefficients of each of these variables and the unit cell CTE. The correlation coefficient is a measure of the linear dependence between two variables.

Table 1 shows the correlation of unit cell CTE with the six parameters. As expected, the strongest correlation is observed with the CTE's of the constituents. However, while theoretical work predicts that the unit cell thermal expansion depends equally on the CTE of the constituents, our sensitivity analysis shows a much stronger correlation on the CTE of the frame. This is likely attributed to the relatively large width of the frame which the theory does not take into account. Also strong correlation of the unit cell CTE is observed on the width of the frame. The Young's moduli of the two materials and the contact area between them do not have a strong correlation with the CTE.

Since α_1, α_2, and the frame width (f_{width}) are the most important parameters influencing the CTE of this metastructure, we conducted a series of full 3D FEM simulations to determine the effect of these variables on the CTE. Statistics programming language R [22] was used to produce a multivariate fit of the CTE on those three variables (equation (2)). The multivariate fit performed is a linear, least squares regression and results in an expression of the unit cell CTE as a linear function of three parameters.

$$\alpha = -4.263 + 1.689\,\alpha_1 - 0.646\,\alpha_2 + 87.945 f_{width} \qquad (2)$$

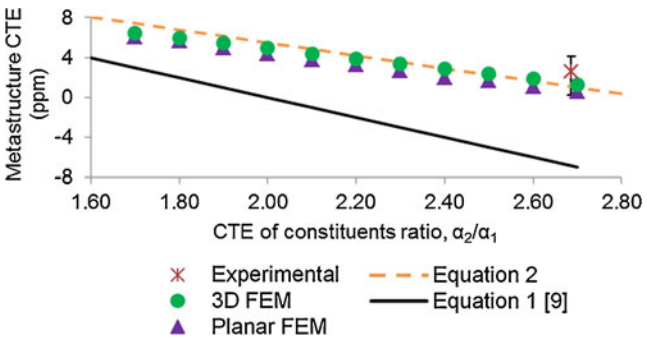

Fig. 8 A comparison for the CTE prediction between equation (1) (*solid line*), equation (2) (*dashed line*), the planar FEM (*triangular symbols*) and 3D FEM (*circular symbols*) models developed in this work, and experimental results (*star symbol*), for various values of CTE of constituents ratio α_2/α_1

In equation (2), α_1 and α_2 are in ppm, f_{width} is in μm/μm, and the output α is expressed in ppm/°C.

Figure 8 presents a comparison between the CTE predictions of equation (1), equation (2) and the planar and 3D FEM models developed in this work, and our experimental results.

Equation (2) was designed for the range $2.3\leq\alpha_2/\alpha_1\leq3.6$. However, equation (2) performs well at the boundary $\alpha_2/\alpha_1=1$ for $\alpha_2=\alpha_1=23.1$ (11 % error) and $\alpha_2=\alpha_1=8.6$ (22 % error). As seen in Fig. 8, equation (2) agrees well with computational and experimental results in this work. Using equation (2) we can thus tune the CTE of our samples by varying three parameters: the CTE's of the constituents and the width of the frame. We can utilize the strong sensitivity of the frame's width to make coarse adjustments to the unit cell CTE, while making finer adjustments through the CTE of the plate and frame. This enables the design of metastructures with a precisely specified CTE.

Table 2 shows the CTE of metastructures that can be achieved by using different metallic constituents and by tuning geometric parameters such as the frame width. Metastructures with a wide range of CTE can be fabricated by using the approach described in this work. This approach can be used to develop even negative CTE metastructures when the ratio of CTE's of the constituents is high enough as in the in the case of the metastructure composed of Kovar (α=5.9 ppm/°C) and Aluminum.

Conclusion

We have demonstrated experimentally the ability to create thin bi-material metastructures exhibiting CTE of 2.6 ppm/°C, significantly lower than that of their constituents (α_1=8.6 and α_2=23.1 ppm/°C). Using 3D finite element analysis, in very good agreement with experiments, we showed the ability to achieve fine and coarse control of the CTE from −3.6 to 8.4 ppm/°C by varying three key parameters (α_1, α_2, and the frame beam width). Finally, we developed a robust fabrication procedure for high aspect ratio thin metallic structures allowing us to easily attempt new designs and ultimately develop large structures of arbitrary CTE. This allows us to design and fabricate thin, thermally stable, high aspect ratio metastructures with tunable CTE. In future work, we aim to test large area lattices and to scale down

this design to thin film scales. We also aim to experimentally show metastructures with a broad range of CTE's, including negative values.

Acknowledgments This work was supported by the Keck Institute for Space Studies at the California Institute of Technology. Part of this research was carried out at the Jet Propulsion Laboratory, California Institute of Technology, under a contract with the National Aeronautics and Space Administration. We thank Jerry Mulder for support with the laser welding process. We also thank Prof. Sergio Pellegrino and Dr. Namiko Yamamoto for valuable advice and assistance, and Prof. Craig A. Steeves for earlier discussions.

References

1. Kuribara K, Wang H, Uchiyama N, Fukuda K, Yokota T, Zschieschang U, Jaye C, Fischer D, Klauk H, Yamamoto T, Takimiya K, Ikeda M, Kuwabara H, Sekitani T, Loo YL, Someya T (2012) Organic transistors with high thermal stability for medical applications. Nat Commun 3:723. doi:10.1038/ncomms1721
2. Roy R, Agrawal DK, Mckinstry HA (1989) Very low thermal-expansion coefficient materials. Annu Rev Mater Sci 19:59–81
3. Ishii J, Akamatsu T (2009) Organo-soluble low CTE polyimides and their applications to photosensitive cover layer materials in flexible printed circuit boards. High Perform Polym 21:123–138. doi:10.1177/0954008308088397
4. Zweben C (1998) Advances in composite materials for thermal management in electronic packaging. JOM 50:47–51. doi:10.1007/s11837-998-0128-6
5. Bollero A, Kaupmees L, Raadik T, Grossberg M, Fernandez S (2012) Thermal stability of sputtered Mo/polyimide films and formation of MoSe2 and MoS2 layers for application in flexible Cu(In, Ga)(Se, S)(2) based solar cells. Thin Solid Films 520:4163–4168. doi:10.1016/j.tsf.2011.04.099
6. Lakes R (1996) Cellular solid structures with unbounded thermal expansion. J Mater Sci Lett 15:475–477
7. Sigmund O, Torquato S (1996) Composites with extremal thermal expansion coefficients. Appl Phys Lett 69:3203–3205
8. Sigmund O, Torquato S (1997) Design of materials with extreme thermal expansion using a three-phase topology optimization method. J Mech Phys Solids 45:1037–1067
9. Steeves CA, Lucato SLDSE, He M, Antinucci E, Hutchinson JW, Evans AG (2007) Concepts for structurally robust materials that combine low thermal expansion with high stiffness. J Mech Phys Solids 55:1803–1822. doi:10.1016/j.jmps.2007.02.009
10. Steeves CA, Mercer C, Antinucci E, He MY, Evans AG (2009) Experimental investigation of the thermal properties of tailored expansion lattices. Int J Mech Mater Des 5:195–202
11. Steeves CA, Evans AG (2011) Optimization of thermal protection systems utilizing sandwich structures with low coefficient of thermal expansion lattice hot faces. J Am Ceram Soc 94:s55–s61. doi:10.1111/j.1551-2916.2011.04447.x
12. Berger J, Mercer C, McMeeking RM, Evansz AG (2011) The design of bonded bimaterial lattices that combine low thermal expansion with high stiffness. J Am Ceram Soc 94:S42–S54. doi:10.1111/j.1551-2916.2011.04503.x
13. Haynes WM (ed) (2009) CRC handbook of chemistry and physics (CRC handbook of chemistry and physics). CRC Press, Taylor and Francis, Boca Raton
14. Patterson K, Pellegrino S, Breckinridge J (2010) Shape correction of thin mirrors in a reconfigurable modular space telescope. Space Telescopes and Instrumentation 2010: Optical, Infrared, and Millimeter Wave 7731 doi:10.1117/12.861442
15. Sutton MA, Wolters WJ, Peters WH, Ranson WF, McNeill SR (1983) Determination of displacements using an improved digital correlation method. Image Vis Comput 1:133–139. doi:10.1016/0262-8856(83)90064-1
16. Chu TC, Ranson WF, Sutton MA (1985) Applications of digital-image-correlation techniques to experimental mechanics. Exp Mech 25:232–244. doi:10.1007/bf02325092
17. FLIR. SC6000 Datasheet. Available: http://www.flir.com/thermography/americas/us/view/?id=44791
18. Brewster MQ (1992) Thermal radiative transfer and properties. Wiley, New York
19. Kaplan H (2007) Practical applications of infrared thermal sensing and imaging equipment, 3rd edn. SPIE Press, Bellingham
20. "Vic2D 2009" (ed) (2009) Columbia, SC: Correlated Solutions, Inc
21. "JMP" (ed) (2007) Cary, NC: SAS Institute Inc
22. Team RC (2012) "R: a language and environment for statistical computing". R. F. f. S. Computing (ed). Vienna, Austria